

# Multi-stage high order semi-Lagrangian schemes for incompressible flows in Cartesian geometries

Alexandre Cameron, Raphaël Raynaud<sup>†</sup>, Emmanuel Dormy<sup>§</sup>

## SUMMARY

Efficient transport algorithms are essential to the numerical resolution of incompressible fluid flow problems. Semi-Lagrangian methods are widely used in grid based methods to achieve this aim. The accuracy of the interpolation strategy then determines the properties of the scheme. We introduce a simple multi-stage procedure which can easily be used to increase the order of accuracy of a code based on multi-linear interpolations. This approach is an extension of a corrective algorithm introduced by Dupont & Liu (2003, 2007). This multi-stage procedure can be easily implemented in existing parallel codes using a domain decomposition strategy, as the communications pattern is identical to that of the multi-linear scheme. We show how a combination of a forward and backward error correction can provide a third-order accurate scheme, thus significantly reducing diffusive effects while retaining a non-dispersive leading error term.

Preprint

## 1. INTRODUCTION

Semi-Lagrangian methods offer an efficient and widely used approach to model advection dominated problems. Initially introduced in atmospheric and weather models [1, 2], these methods are now widely used in all fields of fluid mechanics [3, 4, 5]. They have found a wide range of application in computational fluid dynamics. These methods have triggered a wide variety of schemes, including spline interpolation methods [6, 7, 8], finite element WENO algorithms [9, 10, 11] or CIP methods [12, 13]. Considerable development has also been achieved in application to hyperbolic problems (e.g. compressible hydrodynamics [14], Vlasov equation [15]) and fall out of the scope of this paper.

Semi-Lagrangian methods involve an advected field  $\Phi$ , following the characteristics backward in time. The procedure requires the estimation of field values that do not lie on the computational grid. Semi-Lagrangian methods therefore rely on an interpolation of  $\Phi(t - \Delta t, \mathbf{x} - \mathbf{u}\Delta t)$ , which in general is not a known quantity on the discrete grid.

Because of their local nature, low order semi-Lagrangian methods perform remarkably well on massively parallel computers [16, 17]. Limitations occur with high-order interpolation methods. As the width of the stencil increases, the locality of the scheme is reduced and the resulting schemes require larger communications stencils. When the interpolation strategy is simple, multi-linear in the case of the *CIR* scheme [18], the scheme is local and the computational cost is small. If the interpolation stencil is not localized near the computational point, but near the point where the interpolated value must be reconstructed, one can show that the method is then unconditionally

<sup>†</sup>Current address: School of Astronomy, Institute for Research in Fundamental Sciences (IPM), 19395-5531, Tehran, Iran.

<sup>§</sup>Current address: Département de Mathématiques et Applications, CNRS UMR-8553, École Normale Supérieure, 45 rue d'Ulm, 75005 Paris, France.

stable, in the case of a uniform and steady velocity field [19]. Such schemes are however prone to large inter-process communications, and are not unconditionally stable for general flows.

Dupont *et al.* [20, 21, 22] introduced two new corrective algorithms: “Forward Error Correction” (here denoted *FEC*) and “Backward Error Correction” (here denoted *BEC*). These algorithms take advantage of the reversibility of the advection equation to improve the order of most semi-Lagrangian schemes by using multiple calls of an initial advection scheme. The resulting schemes yield an enhanced accuracy. In that sense, they are built with a similar spirit to the predictor-corrector method [23] or the MacCormack scheme [24].

Here we introduce a new scheme following this methodology, and thus extend this approach to third order accuracy.

## 2. MULTI-STAGE APPROACHES

A possible strategy to increase the order of Semi-Lagrangian schemes is to use higher order interpolation formula e.g. [25]. This has the drawback of relying on a wider stencil, which requires larger communication patterns on a distributed memory computer. Another significant issue with wider stencils is the handling of boundary conditions.

Equation (1) models the advection of a passive scalar  $\Phi$  by a velocity field  $\mathbf{u}$ ,

$$D_t \Phi \equiv [\partial_t + (\mathbf{u} \cdot \nabla)] \Phi = 0. \quad (1)$$

The Lagrangian derivative in (1) is usually defined as the limit, following the characteristic, of

$$D_t \Phi = \lim_{\Delta t \rightarrow 0} \frac{\Phi(t, \mathbf{x}) - \Phi(t - \Delta t, \mathbf{x} - \mathbf{u} \Delta t)}{\Delta t}. \quad (2)$$

Semi-Lagrangian methods rely on this expression to discretize the advective operator  $D_t \Phi$  instead of expanding the sum in a temporal term  $\partial_t \Phi$  and an advective term  $(\mathbf{u} \cdot \nabla) \Phi$ , as in (1). The semi-Lagrangian discretisation of (1) therefore introduces an interpolation operator  $L_{\mathbf{u}}[\Phi^n] = \tilde{\Phi}^n(\mathbf{x} - \mathbf{u} \Delta t)$ , where  $\tilde{\Phi}$  denotes the interpolated value away from the grid points.

A strategy introduced by Dupont *et al.* [20] to increase the order of a semi-Lagrangian scheme, without requiring the use of high-order interpolation formula, is based on two consecutive calls to the interpolation operator, the second call involving the reversed flow. This method is known as the “Forward Error Correction” [20]. The advantages of this procedure over the above high order schemes rely both on the accurate implementation of boundary conditions and on the limited communication stencil. The Forward Error Correction scheme is constructed as

$$\bar{\Phi} \equiv L_{-\mathbf{u}}[L_{\mathbf{u}}[\Phi^n]], \quad (3)$$

$$FEC[\Phi^n] \equiv L_{\mathbf{u}}[\Phi^n] + (\Phi^n - \bar{\Phi})/2. \quad (4)$$

The *FEC* corrective algorithm has further been improved in [21, 22] using three calls to the interpolation operator for each time-step. The resulting algorithm is known as the “Backwards Error Correction” (*BEC*) algorithm. It is constructed using

$$BEC[\Phi^n] \equiv L_{\mathbf{u}}[\Phi^n + (\Phi^n - \bar{\Phi})/2]. \quad (5)$$

Both the *FEC* and the *BEC* algorithms suppress the leading order error term when the interpolation operator is irreversible. Both the *FEC* and the *BEC* schemes are free of numerical diffusion. However, they introduce numerical dispersive effects related to their truncation errors.

This truncation error can be advantageously used to construct a scheme free of numerical dispersion and characterized by a fourth order derivative truncation error. This is achieved for the same computational cost as the *BEC* scheme. A new “Combined Error Correction” (*CEC*) algorithm is introduced, using a linear combination of the *FEC* and *BEC* algorithms,

$$CEC[\Phi] \equiv c_F FEC[\Phi] + c_B BEC[\Phi]. \quad (6)$$

When the *CIR* scheme is used as the interpolation operator, the scheme generated by the *FEC* algorithm is similar, in the Eulerian framework, to the one introduced in [26]. In this case, the values of the coefficients  $c_F$  and  $c_B$  in (6) can be explicitly determined and the stability of the resulting schemes assessed. In one dimension, their expression is

$$3c_F = 2 - \Delta x/(|u|\Delta t) \quad \text{and} \quad c_B = 1 - c_F, \quad (7)$$

where  $\Delta t$  denotes the time-step and  $\Delta x$  the grid-step.

In one dimension of space, the *CIR* scheme is strictly equivalent to the Eulerian upwind scheme. It is well known [27, 28, 29] that this scheme is stable for Courant-Friedrichs-Lewy (CFL) numbers smaller than unity and introduces diffusive errors. The spurious diffusive effects are directly related to the truncation error of the scheme.

The generalization to  $d$ -dimension must be carried out with care. As described later, the fields can be advected one dimension at a time using a splitting technique similar to [26]. In two or three dimensions, the interpolation can be done by applying the *CEC* scheme on each direction separately.

### 3. ONE-DIMENSIONAL ALGORITHMS

In the semi-Lagrangian formalism, the advection equation can be discretized using the *CIR* scheme [18]. In one dimension, the *CIR* scheme has the same stencil as the Upwind scheme [5, 23, 28]

$$\Phi_i^{CIR} = (1 - U_i)\Phi^n[i] + U_i\Phi^n[i - s_i], \quad (8)$$

where  $\Phi^n[i] = \Phi_i^n$  denotes the value of the passive scalar at time  $n\Delta t$  and position  $i\Delta x$ ,  $s_i = \text{sign}(u_i)$  the sign of the velocity and  $U_i = |u_i|\Delta t/\Delta x$  the reduced velocity with  $u_i$  the velocity. A Von Neumann stability analysis shows that the scheme is strictly stable for  $U \leq 1$ . For a constant velocity, the modified equation takes the form

$$\left[ \partial_t \Phi + u \partial_x \Phi \right]_{CIR} = D_{CIR} \partial_x^2 \Phi + \dots \quad \text{with} \quad D_{CIR} = (1 - U) \frac{|u|\Delta x}{2}. \quad (9)$$

The *FEC* scheme (4) is a multi-stage version of the *CIR* scheme. The developed expression for the *FEC* scheme requires the first nearest neighbors for the velocity and the second nearest neighbors for the passive scalar (see Appendix A). For a constant velocity, the expression of *FEC* is

$$FEC[\Phi]_i = -\frac{1}{2}U(1 - U)\Phi^n[i + 1] + (1 - U^2)\Phi^n[i] + \frac{1}{2}U(1 + U)\Phi^n[i - 1]. \quad (10)$$

The stability analysis of (10) provides the following expression for the amplification factor

$$\xi_{FEC} = 1 - U^2 + U^2 \cos(k\Delta x) - iU \sin(k\Delta x). \quad (11)$$

The *FEC* scheme is stable for  $U \leq 1$ . The modified equation associated to this scheme is

$$\left[ \partial_t \Phi + u \partial_x \Phi \right]_{FEC} = -(1 - U^2) \frac{u\Delta x^2}{3!} \partial_x^3 \Phi - 3(1 - U^2) \frac{u^2\Delta x^2\Delta t}{4!} \partial_x^4 \Phi + \dots \quad (12)$$

The *BEC* scheme, presented in (5), is a modified version of the *CIR* scheme using  $\bar{\Phi}^n$  to correct the field before the advection step. The developed expression of the *BEC* scheme requires the second nearest neighbors for the velocity and third nearest neighbors for the passive scalar (see Appendix A). To avoid using this long development, the simplified case of a constant velocity will be studied.

$$\begin{aligned} BEC[\Phi]_i = & -\frac{U}{2}(1 - U)^2\Phi_{i+1}^n + \frac{(1 - U)}{2} (3 - (1 - U)^2 - 2U^2) \Phi_i^n \\ & + \frac{U}{2} (3 - 2(1 - U)^2 - U^2) \Phi_{i-1}^n - \frac{U^2}{2}(1 - U)\Phi_{i-2}^n. \end{aligned} \quad (13)$$

The stability analysis on (13) leads to the following amplification factor

$$\xi_{BEC} = 1 - 2iU \sin(\frac{1}{2}k\Delta x) \left[ e^{-\frac{1}{2}ik\Delta x} U(1 + 2[1 - U] \sin^2(\frac{1}{2}k\Delta x)) + \cos(\frac{1}{2}k\Delta x)(1 - U) \right]. \quad (14)$$

It can be shown analytically that the *BEC* scheme is stable for  $U \leq 1$ . In fact, the *BEC* scheme is still stable for a CFL number smaller than 1.5. The truncation error analysis leads to

$$\begin{aligned} \left[ \partial_t \Phi + u \partial_x \Phi \right]_{BEC} &= - (1 - U)(1 - 2U) \frac{u \Delta x^2}{3!} \partial_x^3 \Phi \\ &\quad - 9(1 - U)^2 \frac{u^2 \Delta x^2 \Delta t}{4!} \partial_x^4 \Phi + \dots \end{aligned} \quad (15)$$

Simulations with Heaviside, triangle and cosine distributions advected by a constant velocity were carried out for a CFL number  $U > 1$ . For  $U \lesssim 1.5$ , the *BEC* scheme gives finite results consistent with the stable results collected for  $U < 1$ . The other schemes (*CIR*, *FEC* and *CEC*) diverge for  $U > 1$  and the *BEC* scheme diverges for  $U \gtrsim 1.5$ . This extension of stability of the *BEC* scheme can be understood in the following way: for  $U > 1$ , the interpolation is performed with points that are not the nearest value to the reconstructed point. The contribution of the second nearest neighbors in the *BEC* formula results in an enhanced stability of the scheme.

The *FEC* and *BEC* schemes both have modified equations with a third order derivative truncation error. The *CEC* scheme, presented in (6) and (7) is a linear combination of these two schemes. The weights are computed to cancel the leading order of truncation error (see Appendix A) and generate a higher order scheme. Using the linearity of the stability analysis, the amplification factor is

$$\begin{aligned} \xi_{CEC} &= 1 - \frac{2}{3} \sin(\frac{1}{2}k\Delta x) \left[ U \left( 3 + 2[1 - U^2] \sin^2(\frac{1}{2}k\Delta x) \right) \sin(\frac{1}{2}k\Delta x) \right. \\ &\quad \left. + \left( 3 + 2U[1 - U^2] \sin^2(\frac{1}{2}k\Delta x) \right) i \cos(\frac{1}{2}k\Delta x) \right]. \end{aligned} \quad (16)$$

The *CEC* scheme is stable for  $U \leq 1$ . To leading order, the modified equation of the *CEC* scheme is

$$\left[ \partial_t \Phi + u \partial_x \Phi \right]_{CEC} = -(1 + U)(1 - U)(2 - U) \frac{|u|(\Delta x)^3}{4!} \partial_x^4 \Phi + \dots \quad (17)$$

The essential properties of the different schemes are reported in Tab. I. The computational cost is evaluated using the number of composed interpolation operators. The complexity of the interpolation operator varies with the interpolation method used. In the case of the *CIR* scheme, the complexity is  $\mathcal{O}(N)$  where  $N$  is the total number grid of points.

Scheme	Formula	Error	Stability	Nb of calls
<i>CIR</i>	$CIR[\Phi] = L_+[\Phi]$	$(1 - U) \frac{ u \Delta x}{2} \partial_x^2 \Phi$	$U < 1$	1
<i>FEC</i>	$FEC[\Phi] = L_+[\Phi] + \frac{1}{2}(\Phi - \bar{\Phi})$	$-(1 - U^2) \frac{u \Delta x^2}{3!} \partial_x^3 \Phi$ $-3(1 - U^2) \frac{u^2 \Delta x^2 \Delta t}{4!} \partial_x^4 \Phi$	$U < 1$	2
<i>BEC</i>	$BEC[\Phi] = L_+[\Phi + \frac{1}{2}(\Phi - \bar{\Phi})]$	$-(1 - U)(1 - 2U) \frac{u \Delta x^2}{3!} \partial_x^3 \Phi$ $-9(1 - U)^2 \frac{u^2 \Delta x^2 \Delta t}{4!} \partial_x^4 \Phi$	$U \lesssim 1.5$	3
<i>CEC</i>	$CEC[\Phi] = L_+[\Phi + \frac{1+U}{6U}(\Phi - \bar{\Phi})]$ $+ \frac{1-2U}{6U}(\Phi - \bar{\Phi})$	$-(1 + U)(1 - U)(2 - U) \frac{ u (\Delta x)^3}{4!} \partial_x^4 \Phi$	$U < 1$	3

Table I. Comparative table of one dimension schemes.

#### 4. RESULTS FOR ONE-DIMENSIONAL PROBLEMS

To assess the efficiency of the schemes introduced previously, simulations with a constant velocity were performed. A one-dimensional periodic domain is considered, and the solution is advected for 10 or 100 cycles. Fig. 1, 2 and 3 show the advection of three density profiles with different regularities. Because of the Fourier properties of sine functions, the first harmonic was studied thoroughly to check that it matches the properties of the modified equation.

The first set of tests was performed using an Heaviside profile  $\Phi(x, t = 0) = \text{sign} \left[ \sin(2\pi x/l) \right]$ . This is a demanding test, as this profile is discontinuous at two cross-over positions (0 and 0.5). As time elapses, the high frequencies get damped and the profile is nearly reduced to its first harmonic. In fig. 1, the *CEC* scheme is closer to the analytical solution than the other schemes by three criteria: (i) the “flatness” of its profile at the beginning of the simulation, (ii) the distance from the analytic cross-over position at all time and (iii) the phase drift of the profile at long time. These criteria may seem independent but they are all linked to the Fourier properties of the modified equation.

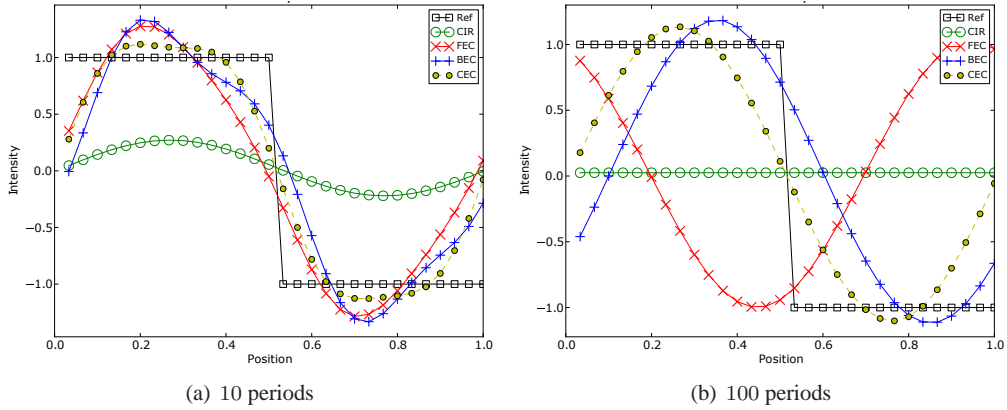


Figure 1. One dimension advection of a Heaviside with a resolution of  $N = 30$  at  $CFL = 0.75$ .

The second set of tests was performed using a triangular profile,  $\Phi(x, t = 0) = |x/l - 0.5|$ . This profile is non differentiable at two cross-over position (0 and 0.5). In fig. 2, the observations reported in the previous paragraph still hold for the triangular profile. As expected, the *CEC* scheme is closer to the analytic results in the case of a continuous but non-derivable profile.

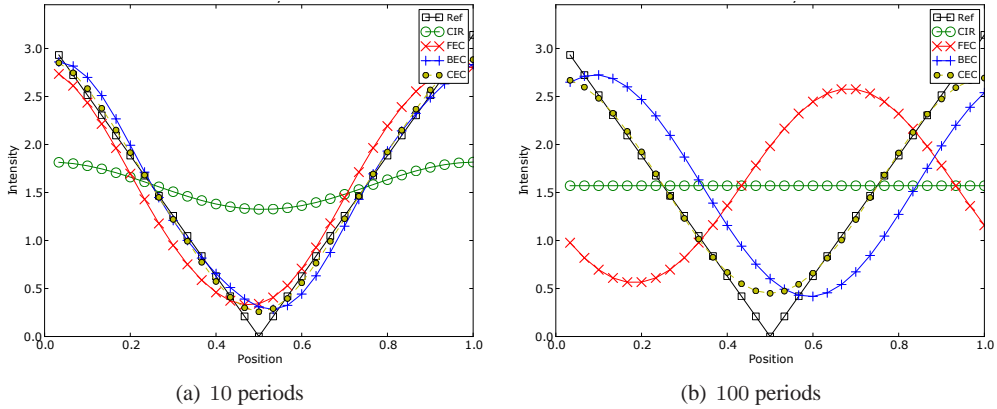


Figure 2. One dimension advection of a triangle with a resolution of  $N = 30$  at  $CFL = 0.75$ .

The last tests were performed using the first harmonic cosine profile,  $\Phi(x, t = 0) = -\cos(2\pi x/l)$ . The properties of the profile will be studied in more details in fig. 9 and 10. In

fig. 3, the *CIR* scheme is so diffusive that a “corrected *CIR*” (green diamond line)\* is plotted. Even though the *CIR* scheme is near zero in fig. 3, the norm of its difference to the analytic profile is smaller than the *FEC* scheme which drifted to such an extent that it is nearly opposite to the reference profile.

As noted above, provided the interpolation strategy involves non-neighboring points, semi-Lagrangian methods can use *CFL* number larger than one. Using a non-local interpolation stencil, we can reproduce the advection test of fig. 3 using a *CFL* number of 3.75, see fig. 4.

The time-step being larger in this last case, fewer time-steps are needed for the same integration time (here respectively 10 and 100 periods), the effects of numerical dispersion and diffusion are thus weakened compared to fig. 3

This is achieved with a simple modification of relations (7) to compute the weights  $c_F$  and  $c_B$  in the form

$$3c_F = 2 - \frac{1}{(|u|\Delta t/\Delta x) \% 1} \quad \text{and} \quad c_B = 1 - c_F, \quad (18)$$

(where  $\%1$  denotes the remainder of the division by unity), the accuracy of the *CEC* scheme is preserved for large *CFL* numbers.

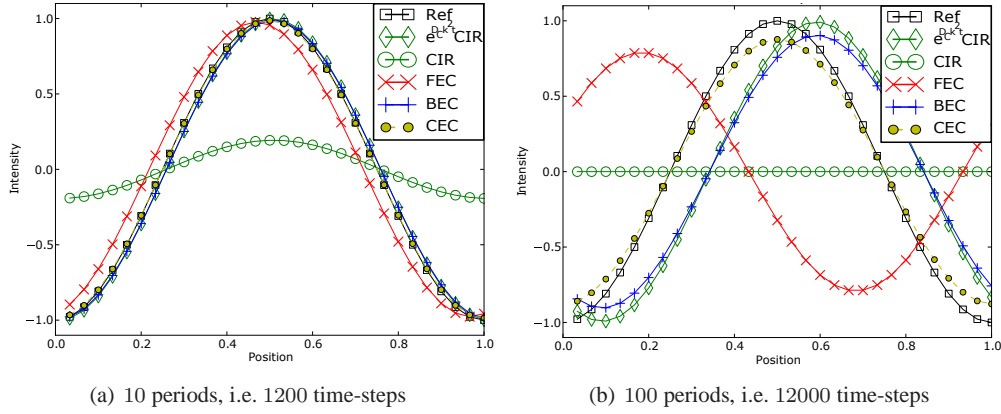


Figure 3. One dimension advection of the cosine function with a resolution of  $N = 30$  at  $CFL = 0.75$ .

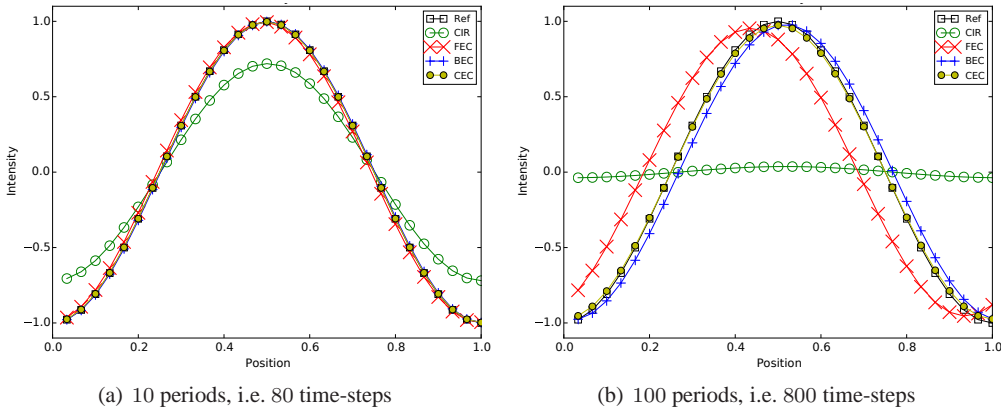


Figure 4. One dimension advection of the cosine function with a resolution of  $N = 30$  at  $CFL = 3.75$ .

\*The corrected *CIR* values are equal to those of *CIR* multiplied by  $\exp(D_{CIR}k^2t)$  where  $D_{CIR}$  is defined in (9).

## 5. MULTI-DIMENSIONAL PROBLEMS

The extension of the above procedures to multi-dimensional problems requires some care. For instance in two dimensions, the *CIR* scheme is

$$\begin{aligned} CIR[\Phi]_{i,j} = & (1 - U_{i,j}^x)(1 - U_{i,j}^y)\Phi_{i,j}^n + (1 - U_{i,j}^x)U_{i,j}^y\Phi_{i,j-s_{i,j}^y}^n, \\ & + U_{i,j}^x(1 - U_{i,j}^y)\Phi_{i-s_{i,j}^x,j}^n + U_{i,j}^xU_{i,j}^y\Phi_{i-s_{i,j}^x,j-s_{i,j}^y}^n. \end{aligned} \quad (19)$$

The semi-Lagrangian *CIR* scheme uses one more value ( $\Phi[i - s_{i,j}^x][j - s_{i,j}^y]$ ) than the Eulerian Upwind scheme. However, the *CIR* scheme is very similar to the directionally split Upwind scheme

$$\Phi_{i,j}^* = (1 - U_{i,j}^x)\Phi_{i,j}^n + U_{i,j}^x\Phi_{i-s_{i,j}^x,j}^n, \quad (20)$$

$$\Phi_{i,j}^{**} = (1 - U_{i,j}^y)\Phi_{i,j}^* + U_{i,j}^y\Phi_{i,j-s_{i,j}^y}^*. \quad (21)$$

In the general case in multi-dimension, there is no expression for the  $c_F$  and  $c_B$  coefficients of the *CEC* scheme. It can be extended to any dimension if the scheme is directionnally split as done in (20) and (21). However, if a simple splitting method is used, the approximation is reduced to first order. Special splitting methods, such as Strang splitting [30], are required to increase the order of the total scheme.

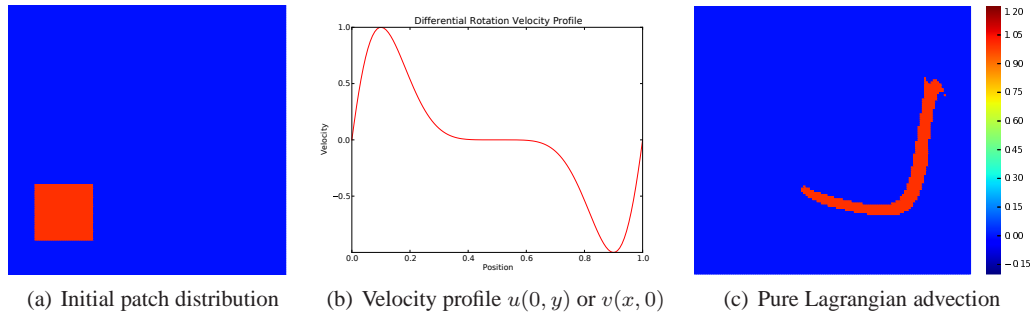


Figure 5. Initial condition, velocity profile and final distribution for the two-dimensional advection test case.

To illustrate applications of our strategy to higher dimensions, let us consider an advection problem in two dimensions of space. A squared patch is considered for the initial distribution of the passive scalar: one inside the square and zero outside, as presented in fig. 5(a). The order of the schemes for regularly varying velocities should be the same as the one for constant velocities. Quantitative results being difficult, only qualitative observations will be made. The following velocity field was used to test the schemes

$$u(x, y) = \frac{y}{l} \left(1 - \frac{y}{l}\right) \left(\frac{1}{2} - \frac{y}{l}\right) \left[ \cos \left(2\pi \frac{y}{l} \left(1 - \frac{y}{l}\right)\right) + 1 \right] / (2\pi^2), \quad (22)$$

$$v(x, y) = -\frac{x}{l} \left(1 - \frac{x}{l}\right) \left(\frac{1}{2} - \frac{x}{l}\right) \left[ \cos \left(2\pi \frac{x}{l} \left(1 - \frac{x}{l}\right)\right) + 1 \right] / (2\pi^2), \quad (23)$$

where  $l$  is the length of the box in both directions. In fig. 5(b), the velocity cancels out on the edges of the box and is divergence free. With the profiles used, the patch is not transported through the walls of the box even though the simulation has periodic boundary conditions. The patch never intersects itself which makes it easier to track. To compare the results, a fully Lagrangian method was used as a reference. The time-step of this method was twenty times smaller to have more accurate results. The solution is represented in fig. 5(c).



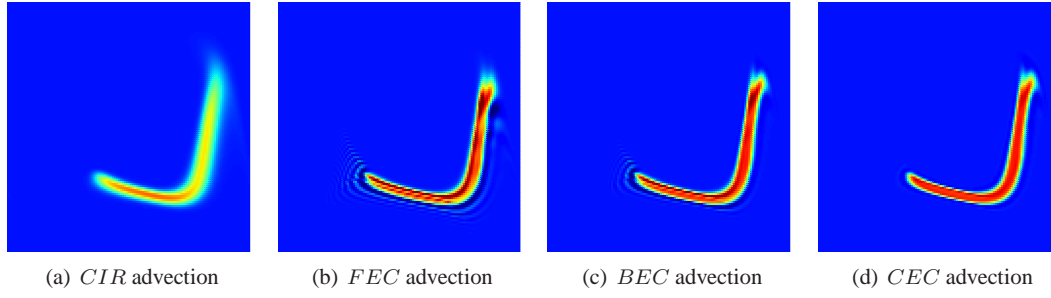


Figure 6. Two-dimensional patch advection using the different schemes.

In fig. 6 and 7, the analysis of the gap between a scheme and the reference solution should not only be guided by the intensity of the difference but also by the area impacted. The *CIR* scheme clearly introduces the largest computational error.

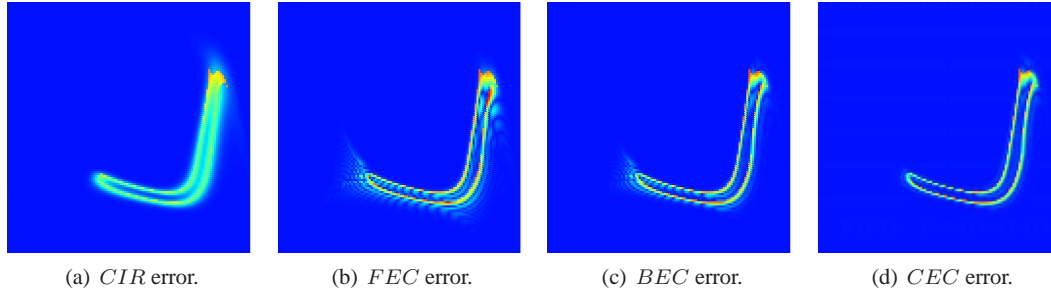


Figure 7. Error, as measured by the difference of the numerical solutions to the reference solution obtained with pure Lagrangian advection.

The perturbation of the distribution can also give an intuition of the leading error term in the modified equation. The quick oscillations at the tail of the patch in fig. 7(b) and 7(c) can be related to the dispersive residuals of the *FEC* and *BEC* schemes. In fig. 7(d), the *CEC* solution is the closest to the reference solution obtained by the pure Lagrangian method. The error is of small amplitude and only impacts the edges of the patch.



## 6. APPLICATION TO THERMAL CONVECTION

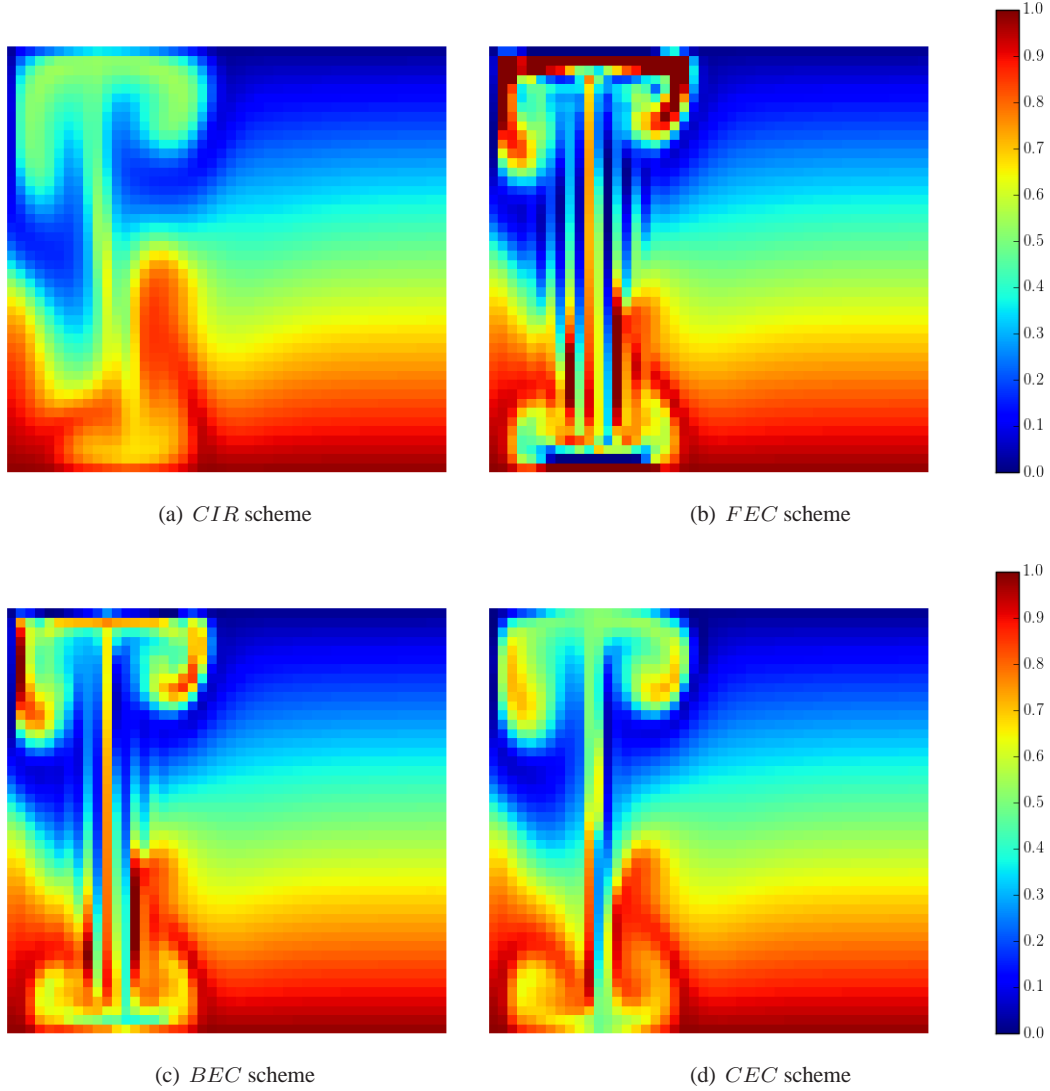


Figure 8. Rayleigh-Bénard evolution of a localized thermal perturbation. The numerical resolution  $N = 50^2$  is intentionally modest, in order to highlight numerical errors.

In this section, the comparison between the different advection schemes is extended to a physically more relevant case: thermal convection in a layer of fluid heated from below. This canonical example is also known as the Rayleigh-Bénard setup. The schemes will not only be used on passive scalars that do not influence the velocity, but on the velocity itself and the temperature, which, in the Rayleigh-Bénard instability, modifies the velocity actively.

The system of equations describing the evolution of the velocity  $\mathbf{u}$  and the temperature  $T$  of the fluid is solved on a two-dimensional Cartesian domain of aspect ratio  $\chi = L_z/L_x = 0.5$ , bounded by solid and impermeable walls. The bottom and top plates are maintained at fixed temperatures  $T_0$  and  $T_0 - \Delta T$ , respectively, whereas the vertical walls are assumed to be insulating (no heat flux through the vertical boundaries). Gravity is assumed to be uniform and vertical  $\mathbf{g} = -g\mathbf{e}_z$ .

To retain the essential physics with a minimum complexity, the Boussinesq approximation is used to describe the fluid within the cell and assume that variations of all physical properties other than

density can be ignored. Variations in density are also neglected “except in so far as they modify the action of gravity” [31]. The density  $\rho$  is assumed to be constant everywhere in the governing equations except in the buoyancy force where it is assumed to vary linearly with temperature,  $\rho(T) = \rho_0 (1 - \alpha (T - T_0))$ , where  $\alpha$  is the thermal expansion coefficient of the fluid.

The system admits the stationary diffusive solution:  $\mathbf{u}^* = 0$ ,  $T^* = T_0 - z \Delta T / L_z$ , and  $\nabla P^* = -g\rho(T^*) \mathbf{e}_z$ . Subtracting the stationary solution, choosing  $L_z$ ,  $L_z^2/\kappa$ , and  $\Delta T$  as units of length, time, and temperature, respectively, and using the temperature perturbation  $\theta = T - T^*$ , the system can be written [32] as

$$\partial_t \mathbf{u} + (\mathbf{u} \cdot \nabla) \mathbf{u} = -\nabla \Pi + \text{RaPr} \theta \mathbf{e}_z + \text{Pr} \nabla^2 \mathbf{u}, \quad (24)$$

$$\partial_t \theta + (\mathbf{u} \cdot \nabla) \theta = w + \nabla^2 \theta, \quad (25)$$

$$\nabla \cdot \mathbf{u} = 0, \quad (26)$$

with  $w \equiv \mathbf{u} \cdot \mathbf{e}_z$  the vertical velocity. The non-dimensional control parameters are the Rayleigh number, defined by  $\text{Ra} = \alpha g \Delta T L_z^3 / (\kappa \nu)$  and which measures the convective driving, and the Prandtl number, defined as the ratio of viscous to thermal diffusion,  $\text{Pr} = \nu / \kappa$ , with  $\nu$  the kinematic viscosity,  $\kappa$  the thermal diffusivity.

Equations (24) and (25) are discretized on a uniform grid using finite volume formula of order two in space and order one in time, with all the terms being treated explicitly. To enforce the solenoidal constraint (26), the pressure-correction scheme [33, 34] is used. This splitting method is composed of two steps. In the first step, a preliminary velocity field  $\mathbf{u}^*$  is computed by neglecting the pressure term in Navier-Stokes equation. Since this preliminary velocity field is generally not divergence-free, it is then corrected in a second step by a projection on the space of solenoidal vector fields. Given the temperature and velocity distributions at time-step  $n$ , the velocity  $\mathbf{u}^{n+1}$  is computed by solving

$$\mathbf{u}^{(1)} = L[\mathbf{u}^n, \mathbf{u}^n], \quad (27)$$

$$\mathbf{u}^{(2)} = \mathbf{u}^{(1)} + \Delta t (\text{RaPr} \theta^n \mathbf{e}_z + [\nabla^2 \mathbf{u}]^n), \quad (28)$$

$$\nabla^2 \phi^n = \nabla \cdot \mathbf{u}^{(2)}, \quad (29)$$

$$\mathbf{u}^{n+1} = \mathbf{u}^{(2)} - \nabla \phi^n. \quad (30)$$

In (29), the algorithm requires to solve at each time-step a Poisson equation for the pressure. The necessary impermeability conditions for the field  $\phi$  are found by multiplying (30) by the normal vector  $\mathbf{n}$ . Together with the velocity boundary condition, they lead to  $\mathbf{n} \cdot \nabla \phi^n = 0$ . The boundary conditions for the velocity field are no-slip, i.e.  $\mathbf{u} = 0$ , while the temperature satisfies  $\theta(z=0) = \theta(z=1) = 0$  on the horizontal boundaries, and  $\partial_x \theta = 0$  on the vertical boundaries. Boundary conditions are imposed on the intermediate velocity field  $\mathbf{u}^*$  by introducing ghost points outside of the domain. In consequence, the tangential component of the actual velocity field  $\mathbf{u}$  will not exactly satisfy the boundary conditions (the error being controlled by the time-step).

In order to develop the instability (the Rayleigh number being sufficiently large and the Prandtl number set to unity), the simulations were always started with  $\mathbf{u} = 0$  and with a small temperature perturbation. This temperature perturbation consisted of a hot spot ( $\theta = 0.1$ ) next to a cold spot ( $\theta = -0.1$ ). This perturbation, localized close to the lower left corner, generates a rising and a sinking plume. The different simulations were compared when the rising plume has reached the top boundary (after roughly a thousand iterations).

A very low resolution,  $N = 50^2$ , was deliberately chosen in order to highlight the numerical errors associated to the different schemes. Snapshots of the total temperature  $T = T^* + \theta$  associated with the thermal plume are compared on figure 8. In fig. 8(b) and 8(c), strong ripples appear in the wake of the plumes. They are not physically relevant and are characteristics of dispersive schemes. The comparison of the plumes in fig. 8(a) and fig. 8(d) clearly highlights that the *CEC* scheme is less diffusive than the *CIR* scheme for practical physical applications. The *CEC* scheme offers an improved scheme, with significantly reduced diffusive effects, and free of the strong dispersion characterizing the *FEC* and *BEC* schemes.

## 7. CONCLUSION

Using the simplest semi-Lagrangian *CIR* scheme introduced by Courant-Isaacson-Rees, it has been demonstrated that a simple multi-stage approach can increase the order of the scheme from first to third order. The resulting scheme is, at leading order, non-dispersive. This procedure was shown to yield significant improvement on a thermal convection problem. It can easily be used to increase the order of existing codes on parallel computers, as the communication stencil is unaltered by the multi-stage approach. The communications among parallel processes are then restricted to the strict minimum (one layer of cell at each domain boundary).

The *CEC* algorithm, introduced here, only requires a modest increase in the computational cost and can easily be implemented in existing codes. Moreover, its implementation is not limited to regular Cartesian finite differences schemes. It can be generalized to other geometries and scheme types by following two simple steps: (i) deriving the modified advection equation for the *FEC* and *BEC* schemes and (ii) combining both schemes to cancel out their leading order error.

## References

1. Robert A. A stable numerical integration scheme for the primitive meteorological equations. *Atmosphere-Ocean* Mar 1981; **19**(1):35–46, doi:10.1080/07055900.1981.9649098.
2. Robert A. A semi-Lagrangian and semi-implicit numerical integration scheme for the primitive meteorological equations. *J. Meteor. Soc. Japan* 1982; **60**(1):319–325.
3. Staniforth A, Côté J. Semi-Lagrangian Integration Schemes for Atmospheric Models A Review. *Mon. Wea. Rev.* Sep 1991; **119**(9):2206–2223, doi:10.1175/1520-0493(1991)119<2206:SLISFA>2.0.CO;2.
4. Oliveira A, Baptista AM. A comparison of integration and interpolation Eulerian-Lagrangian methods. *Int. J. Numer. Meth. Fluids* 1995; **21**(3):183–204, doi:10.1002/flid.1650210302.
5. Durran DR. *Numerical methods for wave equations in geophysical fluid dynamics*. 32, Springer, 1999.
6. Knorr G, Mond M. The representation of shock-like solutions in an Eulerian mesh. *Journal of Computational Physics* Nov 1980; **38**(2):212–226, doi:10.1016/0021-9991(80)90053-4.
7. Shoucri MM. Numerical calculations of discontinuities by shape preserving splines. *Journal of Computational Physics* Feb 1983; **49**(2):334–341, doi:10.1016/0021-9991(83)90130-4.
8. Zerroukat M, Wood N, Staniforth A. Application of the parabolic spline method (PSM) to a multi-dimensional conservative semi-Lagrangian transport scheme (SLICE). *Journal of Computational Physics* Jul 2007; **225**(1):935–948, doi:10.1016/j.jcp.2007.01.006.
9. Liu XD, Osher S, Chan T. Weighted Essentially Non-oscillatory Schemes. *Journal of Computational Physics* Nov 1994; **115**(1):200–212, doi:10.1006/jcph.1994.1187.
10. Qiu JM, Shu CW. Conservative high order semi-Lagrangian finite difference WENO methods for advection in incompressible flow. *Journal of Computational Physics* Feb 2011; **230**(4):863–889, doi:10.1016/j.jcp.2010.04.037.
11. Huang CS, Arbogast T, Qiu J. An Eulerian-Lagrangian WENO finite volume scheme for advection problems. *Journal of Computational Physics* Jun 2012; **231**(11):4028–4052, doi:10.1016/j.jcp.2012.01.030.
12. Nakamura T, Tanaka R, Yabe T, Takizawa K. Exactly Conservative Semi-Lagrangian Scheme for Multi-dimensional Hyperbolic Equations with Directional Splitting Technique. *Journal of Computational Physics* Nov 2001; **174**(1):171–207, doi:10.1006/jcph.2001.6888.
13. Xiao F, Yabe T. Completely Conservative and Oscillationless Semi-Lagrangian Schemes for Advection Transport. *Journal of Computational Physics* Jul 2001; **170**(2):498–522, doi:10.1006/jcph.2001.6746.
14. Lentine M, Grtarsson JT, Fedkiw R. An unconditionally stable fully conservative semi-Lagrangian method. *Journal of computational physics* 2011; **230**(8):2857–2879.
15. Sonnendrücker E, Roche J, Bertrand P, Ghizzo A. The semi-Lagrangian method for the numerical resolution of the Vlasov equation. *Journal of computational physics* 1999; **149**(2):201–220.
16. Liu Y, Liu X, Wu E. Real-time 3d fluid simulation on GPU with complex obstacles. *12th Pacific Conference on Computer Graphics and Applications, 2004. PG 2004. Proceedings, 2004*; 247–256, doi:10.1109/PCCGA.2004.1348355.
17. Wu E, Liu Y, Liu X. An improved study of real-time fluid simulation on GPU. *Comp. Anim. Virtual Worlds* 2004; **15**(3-4):139–146, doi:10.1002/cav.16.
18. Courant R, Isaacson E, Rees M. On the solution of nonlinear hyperbolic differential equations by finite differences. *Comm. Pure Appl. Math.* 1952; **5**(3):243–255, doi:10.1002/cpa.3160050303.
19. Leonard BP. Stability of explicit advection schemes. The balance point location rule. *Int. J. Numer. Meth. Fluids* Feb 2002; **38**(5):471–514, doi:10.1002/flid.189.
20. Dupont TF, Liu Y. Back and forth error compensation and correction methods for removing errors induced by uneven gradients of the level set function. *Journal of Computational Physics* 2003; **190**(1):311 – 324, doi: http://dx.doi.org/10.1016/S0021-9991(03)00276-6.
21. Dupont TF, Liu Y. Back and forth error compensation and correction methods for semi-lagrangian schemes with application to level set interface computations. *Mathematics of Computation* 2007; **76**(258):pp. 647–668.
22. Kim B, Liu Y, Llamas I, Rossignac J. Advections with significantly reduced dissipation and diffusion. *IEEE transactions on visualization and computer graphics* JAN-FEB 2007; **13**(1):135–144, doi:{10.1109/TVCG.2007.3}.

23. Butcher JC. *Numerical methods for ordinary differential equations*. John Wiley & Sons, 2008.
24. MacCormack R. The Effect of Viscosity in Hypervelocity Impact Cratering. *Journal of Spacecraft and Rockets* Sep 2003; **40**(5):757–763, doi:10.2514/2.6901.
25. Celledoni E, Kometa BK, Verdier O. High Order Semi-Lagrangian Methods for the Incompressible NavierStokes Equations. *J Sci Comput* Mar 2015; :1–25doi:10.1007/s10915-015-0015-6.
26. Fromm JE. A method for reducing dispersion in convective difference schemes. *Journal of Computational Physics* Oct 1968; **3**(2):176–189, doi:10.1016/0021-9991(68)90015-6.
27. Courant R, Friedrichs K, Lewy H. ber die partiellen Differenzengleichungen der mathematischen Physik. *Math. Ann.* Dec 1928; **100**(1):32–74, doi:10.1007/BF01448839.
28. Hirsch C. *Numerical Computation of Internal and External Flows: The Fundamentals of Computational Fluid Dynamics: The Fundamentals of Computational Fluid Dynamics*. Butterworth-Heinemann, 2007.
29. LeVeque RJ. *Numerical methods for conservation laws*, vol. 132. Springer, 1992.
30. Strang G. On the Construction and Comparison of Difference Schemes. *SIAM J. Numer. Anal.* Sep 1968; **5**(3):506–517, doi:10.1137/0705041.
31. Rayleigh L. Lix. on convection currents in a horizontal layer of fluid, when the higher temperature is on the under side. *Philosophical Magazine Series 6* 1916; **32**(192):529–546, doi:10.1080/14786441608635602.
32. Chandrasekhar S. *Hydrodynamic and Hydromagnetic Stability*. Dover Books on Physics Series, Dover Publications, 1961.
33. Chorin AJ. Numerical Solution of Navier-Stokes Equations. *Mathematics of Computation* 1968; **22**(104):745–&, doi:10.2307/2004575.
34. Guermond J, Mineev P, Shen J. An overview of projection methods for incompressible flows. *Computer Methods in Applied Mechanics and Engineering* 2006; **195**(4447):6011 – 6045, doi:http://dx.doi.org/10.1016/j.cma.2005.10.010.

## A. DEVELOPED EXPRESSIONS OF THE CORRECTIVE SCHEMES

The expressions relevant to (10) and (13) can be developed as

$$2 \text{FEC}[\Phi]_i = -U_i(1 - U_i)\Phi_{i+s_i}^n + (2 - U_i U_i)\Phi_i^n - U_i U_{i+s_i}\Phi^n[i + s_i - s(i + s_i)] + U_i(1 + U_{i-s_i})\Phi_{i-s_i}^n, \quad (31)$$

$$\begin{aligned} 2 \text{BEC}[\Phi]_i &= (f\Phi^n)[i + s(i)] + (f\Phi^n)[i] + (f\Phi^n)[i - s(i) + s(i - s(i))] + \\ &\quad (f\Phi^n)[i + s(i) - s(i + s(i))] + \\ &\quad \left[ (f\Phi^n)[i - s(i)] + (f\Phi^n)[i - s(i) + s(i + s(i)) - s(i - s(i) + s(i - s(i)))) \right] + \\ &\quad (f\Phi^n)[i - s(i) - s(i - s(i))], \end{aligned} \quad (32)$$

where

$$f[i + s(i)] = -(1 - U_i)U_i(1 - U_{i+s(i)}), \quad (33)$$

$$f[i] = (1 - U_i)[3 - (1 - U_i)^2], \quad (34)$$

$$f[i - s(i) + s(i - s(i))] = -U_i U_{i-s(i)}(1 - U_{i-s(i)+s(i-s(i))}), \quad (35)$$

$$f[i + s(i) - s(i + s(i))] = -(1 - U_i)U_i U_{i+s(i)}, \quad (36)$$

$$f[i - s(i)] = U_i[3 - (1 - U_{i-s(i)})^2] - (1 - U_i)((1 - U_i)U_i), \quad (37)$$

$$f[i - s(i) + s(i + s(i)) - s(i - s(i) + s(i - s(i))))] = -U_i U_{i-s(i)} U_{i-s(i)+s(i-s(i))}, \quad (38)$$

$$f[i - s(i) - s(i - s(i))] = -U_i(1 - U_{i-s(i)})U_{i-s(i)}. \quad (39)$$

## B. ANALYSIS OF THE MODIFIED ADVECTION EQUATION

The modified equation stemming from the discretization of the advection equation has in one dimension the general form

$$\partial_t \Phi + u \partial_x \Phi = \sum_{\alpha} C_{\alpha} \partial_x^{\alpha} \Phi, \quad (40)$$

where the  $C_\alpha$  prefactors come from the truncation error in the case of numeric schemes. If the CFL stability condition is met, i.e.  $\Delta t \propto u^{-1} \Delta x$ , with  $\Delta x \propto N^{-1}$ , we have

$$C_\alpha \propto N^{-\alpha+1}. \quad (41)$$

Going into Fourier space for spacial dimensions and Fourier-Laplace space for time,

$$\Phi(x, t) = \int dk e^{\Omega(k)t - ikx} \hat{\Phi}(k, \Omega(k)) \quad \text{where} \quad \Omega(k) = -\sigma(k) + i\omega(k). \quad (42)$$

Thus, the dispersion relation is

$$\Omega(k) = (ik)u + \sum_{\alpha} (-ik)^{\alpha} C_{\alpha}. \quad (43)$$

Using the decomposition introduced in (42), the decay rate and the phase drift can be expressed as

$$\sigma(k) = \sum_p (k^2)^{2p+2} \left( C_{4p+2} - (k^2)^{2p} C_{4p} \right), \quad (44)$$

$$\omega(k) = k \left( u - \sum_p \left( (k^2)^{2p} C_{4p+1} - (k^2)^{2p+1} C_{4p+3} \right) \right). \quad (45)$$

The equation has strictly stable solutions if and only if  $\sigma(k) > 0$ . Because of their dependence on the resolution, the sequence of  $C_{2p}$  is often equivalent to its first term different from zero. The stability reduces to the criterion  $C_\alpha > 0$  if  $\alpha = 4p + 2$  and  $C_\alpha < 0$  if  $\alpha = 4p$ . Using the equation on  $\omega$ , the phase drift can be extracted

$$\phi(k) = \omega(k) - ku = -k \sum_p \left( (k^2)^{2p} C_{4p+1} - (k^2)^{2p+1} C_{4p+3} \right). \quad (46)$$

It is important to note that the procedure introduced in the *FEC* scheme cannot be repeated recursively. In order to highlight this point let us note that for pure advection, reversing time is equivalent to reversing the velocity

$$\partial_{-t} \Phi + u \partial_x \Phi = 0 \quad \Leftrightarrow \quad \partial_t \Phi + (-u) \partial_x \Phi = 0 \quad \Leftrightarrow \quad \partial_t \Phi + u \partial_{-x} \Phi = 0. \quad (47)$$

Going into Fourier space for the spacial dimension

$$\Phi(x, t) = \int dk e^{-ikx} \tilde{\Phi}(k, t), \quad (48)$$

the modified advection equation can be written as

$$\partial_t (\ln \tilde{\Phi})(k, t) = u(ik) + \sum_{\alpha} C_{\alpha} (-ik)^{\alpha}. \quad (49)$$

Reversing the sign of the coordinate,  $x \rightarrow -x$ , is equivalent to reverse the wave vector,  $k \rightarrow -k$  (c.c. for a real field). In order to ensure time reversibility, the following relation should be satisfied

$$\partial_t (\ln \tilde{\Phi})(k, t) = \partial_t (\ln \tilde{\Phi})(-k, -t) = -\partial_t (\ln \tilde{\Phi})(-k, t). \quad (50)$$

This last relation shows that only terms of odd derivative are reversible. The error on  $\tilde{\Phi}$  highlights this observation. It can be evaluated using

$$(\ln \tilde{\tilde{\Phi}})(k, t) = (\ln \tilde{\Phi})(k, t) + 2\Delta t \sum_p C_{2p} (ik)^{2p}. \quad (51)$$

Only terms of even order derivative modify the field and can be detected with this procedure. This property should also be true for the  $C_\alpha$  coefficients when the velocity is reversed. In the case of the *CIR* scheme, the coefficients depend on the sign of the velocity. In the case of the non-ideal advection equation (40), reverting time leads to

$$\partial_t \Phi + (-u) \partial_x \Phi = \sum_p \left( C_{2p+1}(-u) \partial_x^{2p+1} \Phi - C_{2p}(-u) \partial_x^{2p} \Phi \right). \quad (52)$$

Once more, only terms of odd order derivative are reversible.

The decay rate (fig. 9) and the phase drift (fig. 10) were measured for different resolutions. The results are plotted as a function of the resolution on a binary log scale (lb). fig. 9(a) and 10(a) represent the decay rate and the phase drift, respectively. As shown in (41), the prefactors of the derivative terms of the error are proportional to an integer power of the resolution,  $C_\alpha \propto N^{-\alpha+1}$ . The values of  $\alpha$  are in good agreement with the error term of the modified equation. Using the theoretical value of  $\alpha^{(1)}$  and  $\alpha^{(2)}$ , the values are rescaled to  $\phi_{res} = \phi \times N^{\alpha^{(1)}-1}$  and  $\sigma_{res} = \sigma \times N^{\alpha^{(2)}-1}$ . fig. 9(b) and 10(b) show that the rescaled values are nearly constant as predicted by the theory.

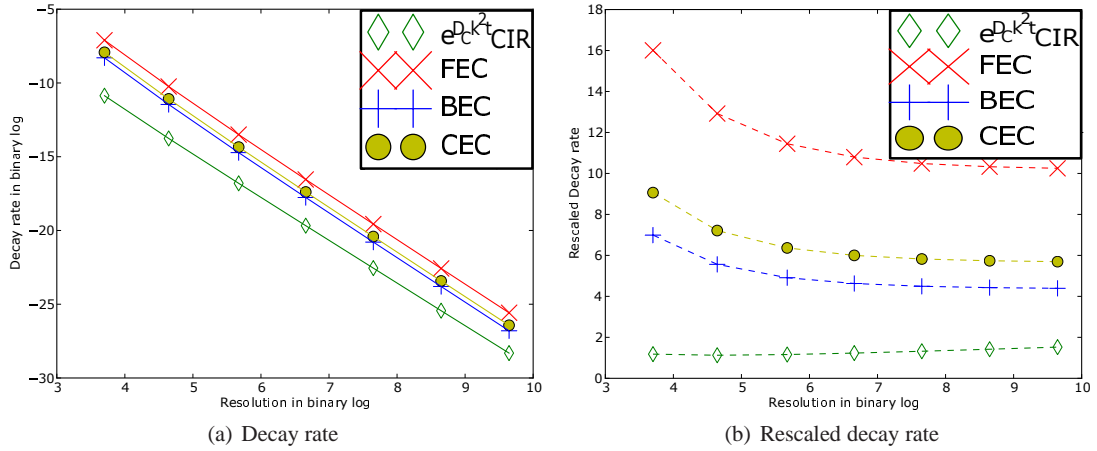


Figure 9. Evolution of the decay rate with the resolution in one dimension.

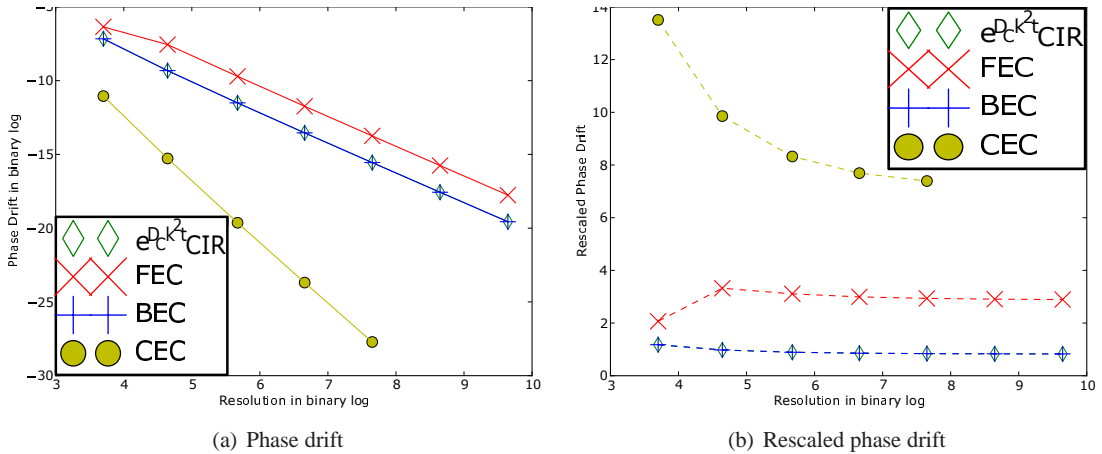


Figure 10. Evolution of the phase drift with the resolution in one dimension.